We are IntechOpen, the world's leading publisher of Open Access books
Built by scientists, for scientists

4,200
Open access books available

116,000
International authors and editors

125M
Downloads

Our authors are among the

154
Countries delivered to

TOP 1%
most cited scientists

12.2%
Contributors from top 500 universities

CLARIVATE ANALYTICS
BOOK CITATION INDEX
INDEXED

WEB OF SCIENCE™

Selection of our books indexed in the Book Citation Index in Web of Science™ Core Collection (BKCI)

Interested in publishing with us?
Contact book.department@intechopen.com

Numbers displayed above are based on latest data collected.
For more information visit www.intechopen.com

Chapter

Cobalt-Based Catalysts for CO Preferential Oxidation

Leticia E. Gómez and Alicia V. Boix

Abstract

In this work, catalysts based on cobalt supported on ZrO_2 and CeO_2 and CoCeMnOx were studied for the CO preferential oxidation (COPrOx) in hydrogen-rich stream able to feed fuel cells. Among them, the CoCeMnOx formulation showed the highest CO conversion at low temperatures, while the cobalt oxide supported on ceria presented the best selectivity toward CO_2. The Co_3O_4 spinel was the active phase for the CO preferential oxidation detected in all catalysts. However, the CoOx-CeO_2 and CoCeMnOx catalysts resulted more active than cobalt oxide supported on zirconia. The presence of ceria close to cobalt species promotes the redox properties and enhances the catalytic activity. In the CoCeMnOx catalyst prepared by coprecipitation, the incorporation of Mn represented an additional positive effect. The presence of Mn promoted the reoxidation of Co^{2+} to Co^{3+} and, consequently, the activity increased at low temperature. By X-ray diffraction (XRD) of CoOx-ZrO_2 and the CoOx-CeO_2 catalysts, the Co_3O_4 spinel and ZrO_2 or CeO_2 were identified in agreement with laser-Raman spectra. At the same time, the CoCeMnOx catalyst, prepared by coprecipitation of precursor salts, showed an incipient development of a new phase $(Mn,Co)_3O_4$ mixed spinel, due to the intimate contact between elements.

Keywords: COPrOx, $(Mn,Co)_3O_4$ mixed spinel, redox couple, CoCeMnOx, CeO_2 support, XPS, laser-Raman spectroscopy

1. Introduction

The global demand for energy has been inexorably growing in the last decades. The increasing use of fossil fuels in order to generate energy causes serious problems to the environment due to the gaseous emissions. This fact has produced a global movement toward trying to remove the contaminants from combustion effluents. Besides, the exploration for alternatives to fossil fuels, biofuels or hydrogen as an energy vector, has gained an immediate and future significance because this could contribute to the depletion of greenhouse gases [1–3].

Fuel cells are devices that are being actively developed, because they are power generation systems that can produce energy with significantly less impact on the environment. Among several types of fuel cells, proton exchange membrane fuel cells (H_2-PEMC) are considered to be the most technically advanced for such application [4]. Hydrogen produced by means of the steam reforming or autothermal process of hydrocarbons or alcohols should contain less than 10 ppm of carbon monoxide before entering the cell since CO poisons the Pt anode of the fuel cells (**Figure 1**) [5, 6]. After the reforming step, the hydrogen production process

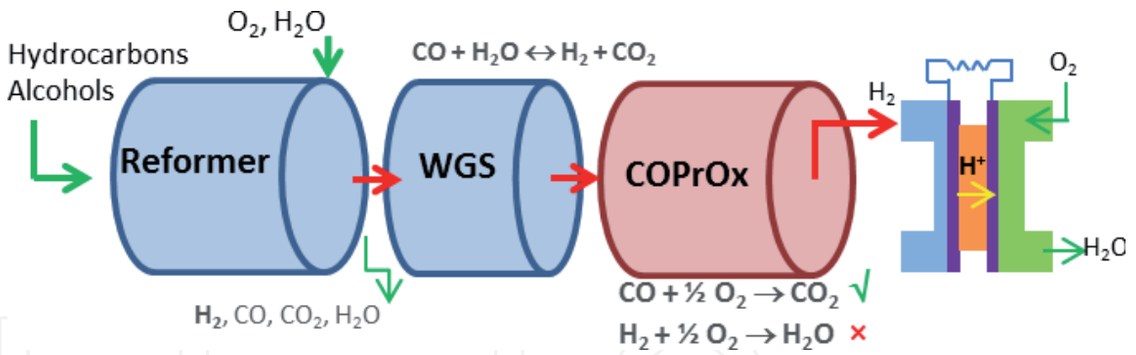

Figure 1.
Schematic flow diagram of a typical fuel cell processor with COPrOx.

continues with the water gas shift reaction (WGSR), where the stream is enriched in hydrogen and the CO content is diminished to 1%. As the CO concentration in the hydrogen stream is so high to enter to the cell, it is necessary to reduce it to the desired levels. Among various methods such as catalytic methanation, Pd-based membrane, and catalytic CO preferential oxidation (COPrOx), the latter is considered as the most adequate due to its simplicity and effectiveness. Thus, given the importance of the hydrogen purification process, the last few years have witnessed the surge of a renewed interest in the CO oxidation reaction, and several contributions dealing with this issue have recently been published [5–7].

In our research group, catalysts for the removal of contaminants from vehicles, industrial facilities, and power-generating sources have been studied [8, 9]. In addition, catalysts and catalytic reactors have also been investigated for the production and purification of H_2 to be used in fuel cells [10–13].

On the other hand, due to their redox properties, cobalt-containing catalysts have been the object of numerous publications in the environmental catalysis field and in the purification of H_2 stream, among other applications. For example, catalysts based on cobalt oxides have been studied for soot combustion [14], NOx selective reduction in oxygen excess [15], and CO preferential oxidation reaction [16].

The challenges involved in the design of successful COPrOx catalysts are the following: (i) high CO oxidation activity at low temperatures, (ii) high selectivity for CO oxidation against the undesired H_2 oxidation, and (iii) good resistance to deactivation caused by the H_2O and CO_2 in the feed [5, 6, 17].

In order to reduce the CO concentration without consuming H_2, several catalysts have been studied with promising results. Catalysts of Pt supported on bimetallic systems achieved excellent results [17–19], but the high cost of noble metals led the investigations toward the use of other active phases. For instance, CuO/CeOx catalysts have shown a catalytic performance in the COPrOx comparable to those based on noble catalysts [20–22].

In this vein, it has been shown that the combined effect of cobalt oxide and ceria strongly influences the morphological and redox properties of the composite oxides, by dispersing the Co_3O_4 phase and promoting the efficiency of the Co^{3+}/Co^{2+} redox couple [23, 24]. Numerous publications have shown that the addition of other metals to a cerium-based mixed oxide (Zr or Mn) increases the oxygen storage capability of the ceria. This effect is originated by the increase in the surface oxygen mobility due to chemical interactions between cobalt, cerium, and other metals [25–27].

On the other hand, the use of structured catalysts as those supported onto honeycomb monoliths has long been considered in the chemical industry, and it has increased with the significance of environmental catalysis in pollution abatement applications due to catalysts with a high attrition resistance and a low pressure drop that are required. In addition the thin catalytic coating allows high efficiency and

selectivity. Cordierite offers high mechanical strength, high resistance to elevated temperatures, and temperature shocks due to its low thermal expansion coefficient. Moreover, it presents great adhesion stability, which is a very important property for the monolithic catalysts [12, 13, 15, 16].

In our previous work with structured catalysts, we showed that cobalt supported on zirconia and ceria and CoCeMnOx mixed oxides resulted in efficient catalysts for the COPrOx. However, it is of great interest both to identify the cobalt species present in an active catalyst and to analyze the interactions with the support (CeO_2 or ZrO_2) and their influence on the catalytic behavior. It is also important to understand the role of cobalt in the CoCeMnOx mixed oxides. In the present work, a very detailed analysis of the species present in these complex systems was carried out. The catalysts were analyzed by X-ray diffraction (XRD) and temperature-programmed reduction (TPR). The X-ray photoelectron spectroscopy (XPS) and laser-Raman spectroscopy (LRS) were used to characterize the oxidation state, concentration, and chemical nature of species present on catalysts.

2. Materials and methods

2.1 Preparation of cobalt-based catalysts

Three main groups of Co-based catalysts with 10 wt.% of cobalt were prepared—CoOx/ZrO_2, CoOx-CeO_2, and CoCeMnOx—in order to study the cobalt species and their relation to the centers active in the CO preferential oxidation.

The CoOx-ZrO_2 catalyst with 10 wt.% cobalt on ZrO_2 was prepared by wet impregnation and labeled CoZ. A commercial zirconia support (6.8 m^2/g, pore volume ca. 0.013 cm^3/g) was impregnated with an aqueous solution of $Co(NO_3)_2$. The mixture was evaporated until achieving a paste, which was placed in the oven overnight at 120°C.

CoOx-CeO_2 catalysts were prepared by two different methods. The CoCe-I sample was produced by the wet impregnation method with 10 wt.% of cobalt, using an aqueous solution of $Co(NO_3)_2$ and CeO_2 powder as support which was obtained by precipitation of the $Ce(NO_3)_3$ solution with $NH_4(OH)$. The mixture was evaporated under continuous agitation until achieving a paste, which was placed in the oven overnight at 110°C. By means of the coprecipitation method, CoCe-P catalyst was obtained. The aqueous solution of $Co(NO_3)_2$ and $Ce(NO_3)_3$ was precipitated with $NH_4(OH)$ added drop by drop under vigorous stirring. The resulting precipitate was filtered and washed several times with distilled water and dried overnight at 110°C.

The CoCeMnOx oxide mixture catalyst with 10 wt.% of Co and Mn/Co molar ratio of 1/4 was prepared by the coprecipitation method, adding $NH_4(OH)$ to an aqueous solution of $Co(NO_3)_2$, $Ce(NO_3)_3$, and $Mn(NO_3)_2$. The mixture was kept 2 h under continuous stirring at room temperature. The precipitate obtained was washed several times with deionized water and then dried overnight at 110°C.

After drying, all obtained solids were calcined for 5 h at 500°C under flowing air (25 mL/min), and the temperature was ramped from room temperature up to 500°C at 10°C/min.

2.2 Characterization

2.2.1 Chemical composition quantification

Elemental analyzes were performed by inductively coupled plasma atomic emission spectroscopy (ICP-AES) on an ICP Optima 2100 DV PerkinElmer instrument.

2.2.2 Surface area measurement

The specific surface area was calculated by BET method from N_2 adsorption isotherms at −196°C with a Micromeritics TriStar 3000 instrument. The powder samples (50 mg) were previously outgassed in vacuum at 300°C for 3 h in order to remove any adsorbed substance. The volume of adsorbed N_2 was measured as the pressure was increased.

The surface area S of the catalysts was calculated as

$$S = \frac{v_m N A}{VM} \tag{1}$$

where N is the Avogadro number, VM is the molar volume of a gas, A is the area of a molecule of nitrogen, and v_m is the volume of an adsorbed monolayer of gas, which is obtained from the BET equation

$$\frac{P}{v(P_0 - P)} = \frac{1}{v_m c} + \frac{(c-1)}{v_m}\frac{P}{P_0} \tag{2}$$

where P and P_0 are the equilibrium and the saturation pressure of N_2 at the temperature of adsorption, v is the adsorbed gas volume, v_m is the volume of an adsorbed monolayer, and c is the BET constant.

2.2.3 X-ray diffraction (XRD)

The patterns of all samples were measured on a Shimadzu XD-D1 instrument with monochromator using Cu-Kα radiation at a scanning rate of 1°/min in the range of 2θ = 20°–80°.

2.2.4 Temperature-programmed reduction (H_2-TPR)

The catalysts (100 mg) were pretreated in Ar flow heating up to 300°C and held 30 min in order to clean the catalytic surface. The reducing gas was a 5% H_2/Ar mixture; the temperature was ramped up at 10°C/min to 900°C. The experiments were carried out using an Okhura TP-2002S instrument equipped with a thermal conductivity detector (TCD). The H_2 uptake was registered as the temperature increased.

2.2.5 Laser-Raman spectroscopy (LRS)

The laser-Raman spectra of catalysts and CeO_2 and ZrO_2 supports disposed as pressed powder were measured with a LabRAM spectrometer (HORIBA Jobin Yvon) with an Olympus confocal microscope, equipped with a charge-coupled device (CCD) detector. The excitation wavelength was in all cases 532 nm. The laser power was set at 30 mW. In addition, a Linkam high-temperature cell was used for the in situ experiments, introducing into the cell 50 mg of powder catalysts. The reductive/oxidative treatments were carried out at different temperatures. The concentration and the caudal of gas reactants which entered to the cell were controlled by mass flow controllers. A thermocouple placed on the middle of the catalytic cell allowed the temperature control.

2.2.6 X-ray photoelectron spectroscopy

XPS analyses were performed in a multi-technique system (SPECS) equipped with AlKα X-ray source and operated at 100 W with pass energy of 30 eV. In

addition, in order to avoid the spectral interference (Mn LMM with Ce 3d), the spectra of Ce 3d, O 1s, and C 1s were measured with MgKα X-ray source. The XPS analyses were performed on the calcined powders which were previously pressed. The data treatment was performed with the Casa XPS program (Casa Software Ltd., UK).

2.3 Assessment of the catalytic activity

CO preferential oxidation experiments were performed in a fixed-bed flow reactor at atmospheric pressure. The reaction mixture consisted of 1% CO, 1% O_2, and 40% H_2 and He balance. The weight/total flow ratio was adjusted to 2.1 mg•min/mL. The CO conversion (X_{CO}) and the oxygen selectivity toward CO_2 (S_{O2}) were defined as

$$X_{CO}(\%) = \frac{\left(C^0_{CO} - C_{CO}\right)}{C^0_{CO}} \times 100 \tag{3}$$

$$S_{O_2}(\%) = 0.5\,\frac{\left(C^0_{CO} - C_{CO}\right)}{\left(C^0_{O_2} - C_{O_2}\right)} \times 100 \tag{4}$$

where C_{CO} and C_{O2} were reactor exit concentrations of CO and O_2, respectively, while $C_{CO}{}^0$ and $C_{O2}{}^0$ represented the feed concentrations. The stream compositions were measured with a chromatograph GC-2014 Shimadzu equipped with a TCD cell. All catalysts were pretreated during 1 h in O_2/He flow at 200°C before the catalytic test. In order to study the stability and a possible deactivation caused by the presence of CO_2, the CoCeMnOx catalyst was tested during 75 h at 175°C, adding 20% CO_2 in the reactant mixture.

3. Results and discussion

3.1 Prepared catalysts

The compositions of the cobalt-based catalysts, analyzed by the ICP technique, are presented in **Table 1** and are in agreement with the predefined nominal values. The cobalt content (wt.%) resulted 9.2, 10.6, and 8.6 for CoZ, CoCe-I, and CoCe-P, respectively, while for the mixture of oxides CoCeMnOx, the concentrations of Co, Mn, and Ce were 11, 2.6, and 24.8 wt.%, respectively.

The BET method was used to determine the surface specific area of each sample, and the values are also reported in **Table 1**. The surface area of the CoZ sample practically did not change with the impregnation of cobalt, showing BET value of 7.5 m^2/g, close to the ZrO_2 support. On the other hand, the surface area was similar for the CoOx-CeO_2 catalysts, regardless of the impregnation or coprecipitation methods used. As it can be observed for CoMnCeOx, the addition of a small amount of manganese increased the specific surface with respect to the other samples, possibly due to the insertion of Mn in the ceria structure.

3.2 X-ray diffraction

The crystalline structures of the different Co-based catalysts and that of the ZrO_2 and CeO_2 supports were analyzed by means of XRD. **Figure 2** shows the diffraction patterns of the samples.

The CoOx-CeO_2 catalysts (CoCe-I and CoCe-P) show patterns dominated by the characteristic CeO_2 diffraction peaks, whose main signals appear at 2θ = 28.6°,

33.4°, 47.8°, and 56.6° (JCPDS34-0394). The peaks of Co_3O_4 at 2θ = 31.3°, 36.8°, 44.8°, 59.4°, and 65.3° (JCPDS 42-1467) do not seem to modify the structure of the CeO_2 diffraction pattern. Despite the different preparation methods that were used, only two phases can be distinguished, i.e., Co_3O_4 spinel and CeO_2 with fluorite structure.

Catalysts	Preparation method	Co (wt.%)	Mn (wt.%)	Molar ratio of Co/ Zr or Ce	BET area (m^2/g)
CoZ	wet impregnation	9.2	—	0.15	7.5
CoCe-I	wet impregnation	10.6	—	0.14	93
CoCe-P	co-precipitation	8.6	—	0.14	92
CoCeMnOx	co-precipitation	11.0	2.6	1.06	165

Table 1.
Co-based catalysts, compositions, and specific surface area.

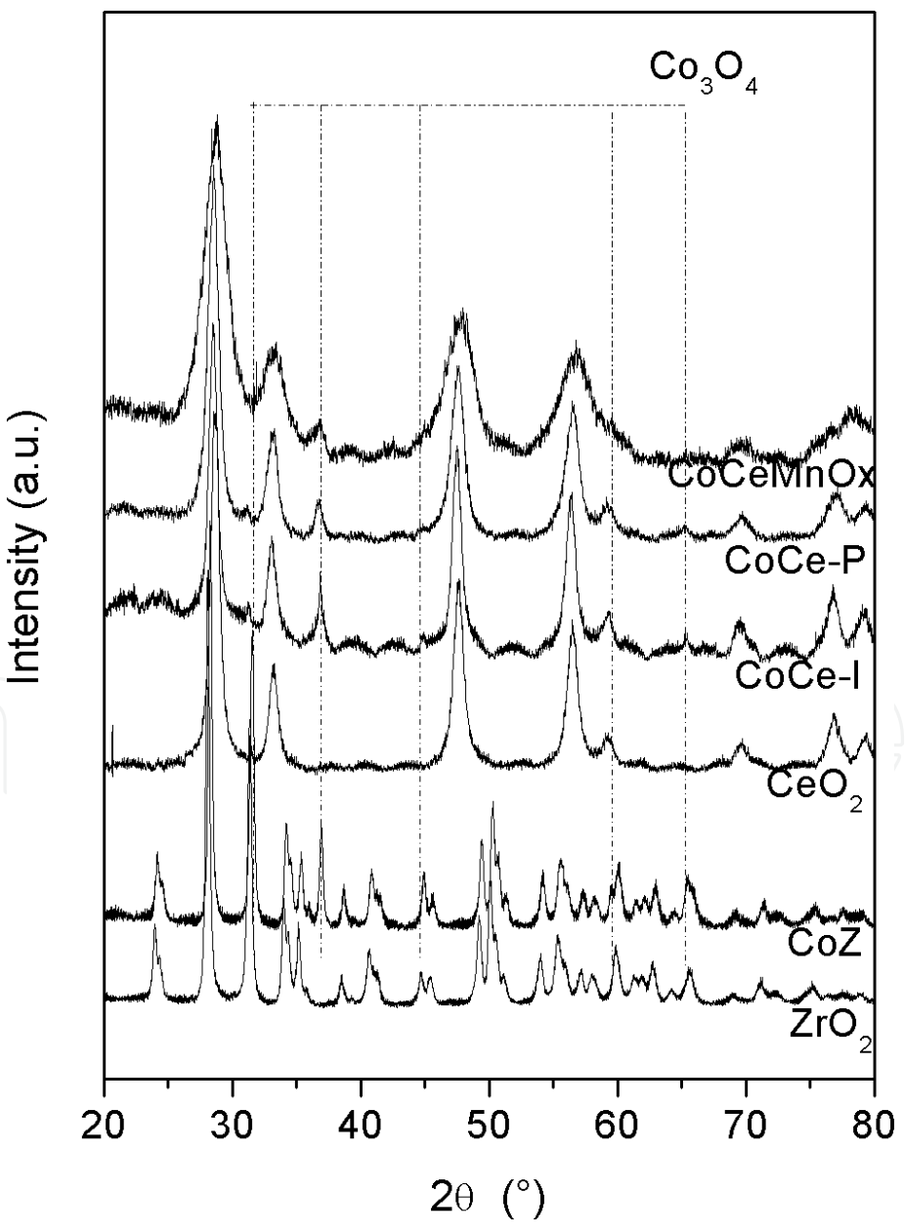

Figure 2.
XRD patterns of CoZ, CoCe-I, CoCe-P, and CoCeMnOx catalysts and CeO_2 and ZrO_2 supports.

On the other hand, the diffraction pattern of the CoZ catalyst shows the peaks associated with the monoclinic ZrO_2 support and the main signal of Co_3O_4 at $2\theta = 36.8°$.

In the diffraction pattern of the CoCeMnOx catalyst, a broadening of peaks corresponding to the CeO_2 phase can be observed. These results could indicate that the structure of CeO_2 is distorted due to the insertion of manganese, although the type fluorite structure of CeO_2 is still maintained [28]. It can be observed that in the main signal of CeO_2 ($2\theta = 28.6°$), an asymmetric broadening appears associated with an incipient formation of the $(Mn,Co)_3O_4$ phase, which has a characteristic peak at 29.4° (JCPDS 18-408). Likewise, the main peak of the $(Mn,Co)_3O_4$ phase ($2\theta = 36.4$) appears at 36.9°, close to the main signal of the Co_3O_4 spinel.

3.3 Temperature-programmed reduction

Figure 3 exhibits the reduction peaks corresponding to cobalt-based catalyst. The reduction profile of the CoZ catalyst presents a peak, whose maximum is at 395°C, and a shoulder, at 370°C. The cobalt oxide reduction is completed at 440°C. It is known that the reduction of Co_3O_4 takes place in two steps that correspond to the subsequent reduction of the Co^{3+} and Co^{2+} species present in the spinel structure.

The CoCe-P profile presents two intense peaks at 300 and 380°C belonging to Co_3O_4 reduction. The small signals at 471 and 850°C could be attributed to the reduction of the ceria support, superficial oxygen, and bulk species, respectively [29, 30]. On the other hand, in the CoCe-I sample, the peak at 471°C is a small shoulder. It is probable that for the coprecipitated catalysts, a more intimate contact between Co and Ce species takes place. This fact produces a synergistic effect promoting the reducibility of the species and the mobility of surface oxygen species in ceria support. The performance of Co_3O_4 phase on COPrOx reaction follows a redox mechanism which involves the reduction/oxidation of the Co^{3+} site. The presence of ceria and the synergism with cobalt would improve its reducibility. According to the H_2 consumption of each sample, the H_2/Co ratio close to 1.33 revealed that Co_3O_4 is the cobalt phase present on CoZ catalysts. In the case of CoOx-CeO_2 catalysts, the H_2/Co ratio values higher than 1.33 were calculated. This would indicate that a CeO_2 fraction was reduced within the range of temperatures studied.

The profile of the CoCeMnOx catalyst shows three reduction zones at low (150–420°C), intermediate (420–620°C), and high (650–900°C) temperatures. As shown by XRD, the Co species seems preferentially to form the Co_3O_4 spinel ($2\theta = 36.9°$) without distortion of the CeO_2 structure, which is reduced at low temperature. The reduction of manganese species should also be considered in this zone, because there are multiple overlapping peaks [28]. Then, the cobalt species (Co_3O_4) and a fraction of the Mn^{4+}/Mn^{3+} species incorporated to the ceria structure might be reduced below 420°C. The reduction temperatures of Co_3O_4 in the CoCeMnOx catalyst are lower than in the CoCe-I and CoCe-P samples. The other broad peak centered at 800°C is a typical reduction peak of bulk CeO_2 and could also be associated with some difficult-to-reduce Mn^{n+} species.

3.4 Laser-Raman spectroscopy

The laser-Raman spectra of catalysts and CeO_2 and ZrO_2 supports are shown in **Figure 4**. The CeO_2 spectrum shows a main band at 464 cm^{-1} (F2g mode) and other weaker signals at 259, 587, and 1173 cm^{-1} belonging to second-order (2 TA, D, and 2TO) Raman modes, respectively, which are associated to oxygen vacancies [31–33].

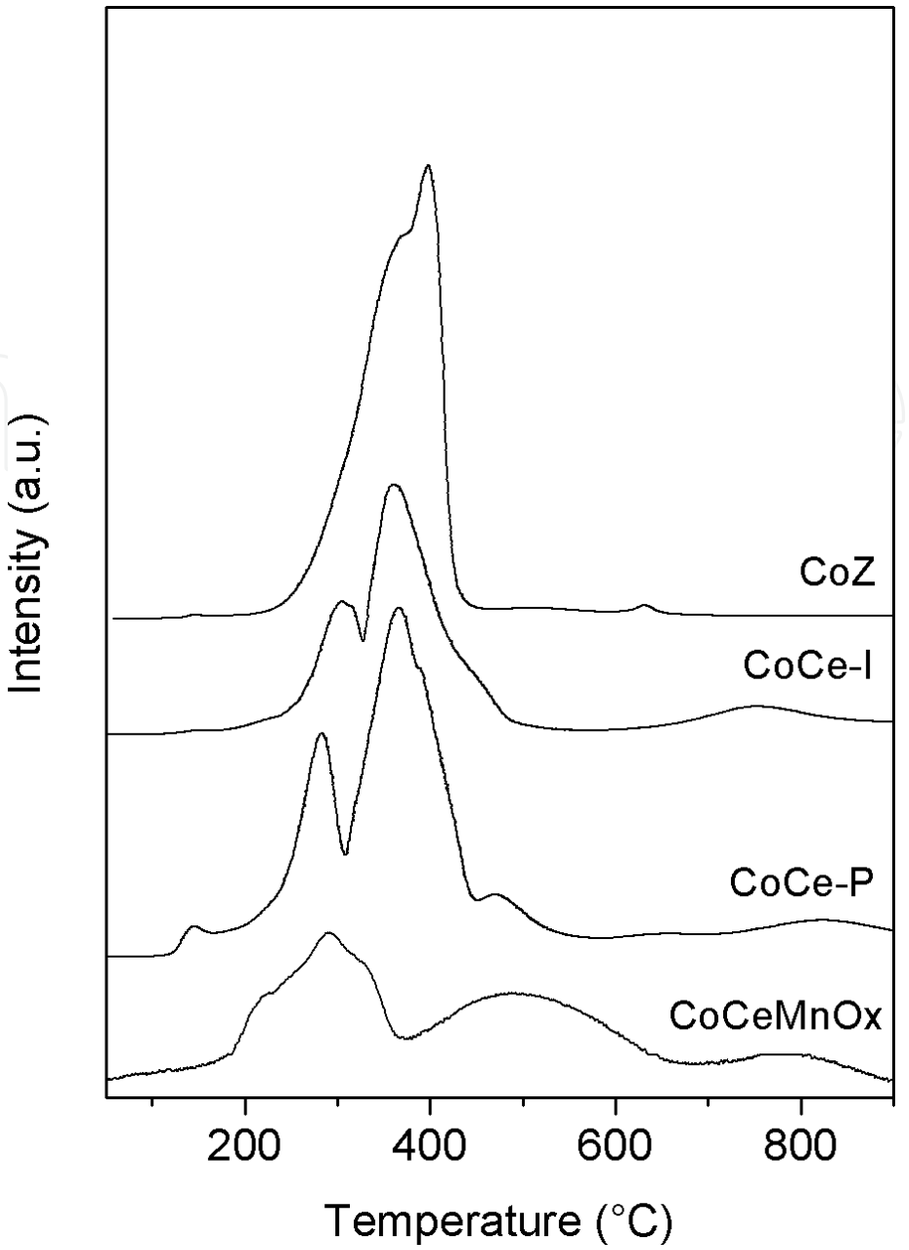

Figure 3.
Temperature-programmed reduction of CoZ, CoCe-I, CoCe-P, and CoCeMnOx catalysts.

The Raman spectra of CoCe-I and CoCe-P show a single peak at 464 cm^{-1}, which corresponds to CeO_2, as well as the signals at 193, 484, 524, 615, and 680 cm^{-1} assigned to the vibrations of the Co_3O_4 spinel. The bands at 193, 524, and 615 cm^{-1} were attributed to the F2g mode, while the bands at 484 and 680 cm^{-1} were assigned to the Eg and A1g modes, respectively [34].

In the CoCeMnOx spectrum, the bands of Co_3O_4 oxide are not detected. However, a small peak at 666 cm^{-1} is observed, due to the possible formation of a Mn,Co mixed spinel. Nevertheless, the XRD patterns showed the main peak corresponding to the Co_3O_4 spinel Therefore, the co-existence of Co_3O_4 and $(Mn,Co)_3O_4$ phases could also be possible.

The Raman spectra of the CoZ catalysts and ZrO_2 support are shown in **Figure 4**. The main bands at 680 and 520 cm^{-1} can be observed corresponding to cobalt oxides [35]. The other bands at 193, 475, and 615 cm^{-1} overlap with the bands of zirconia monoclinic phase.

In order to understand the change of the active phase under different atmospheres, the CoCe-I catalyst was subjected to different reductive/oxidative

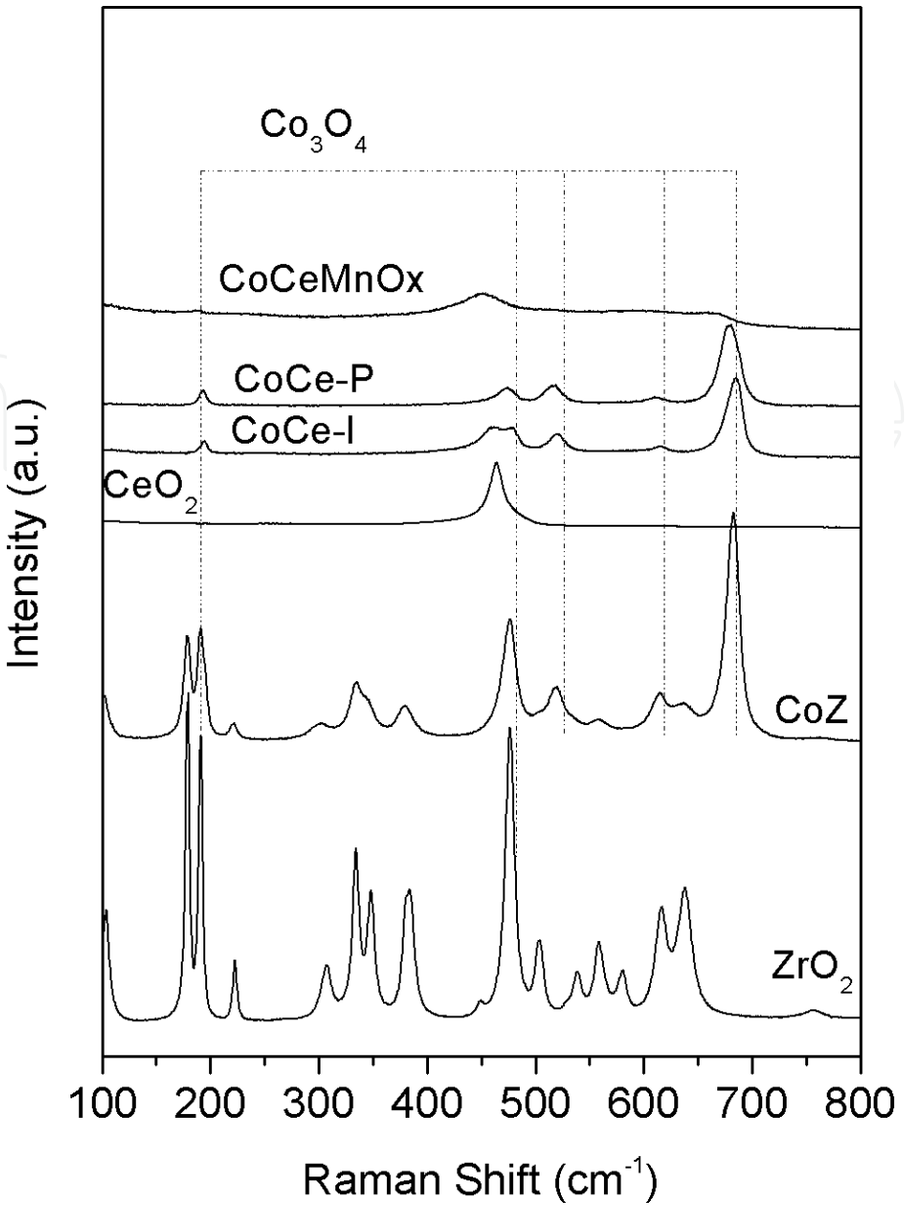

Figure 4.
Raman spectra of CoZ, CoCe-I, CoCe-P, and CoCeMnOx catalysts.

treatments at different temperatures. These experiments were followed by in situ Raman spectroscopy, recording spectra at each temperature. The catalyst was placed in a reaction chamber coupled to the spectrometer.

The first experiment consisted in reducing the catalysts with a 1% CO/Ar stream with the purpose of analyzing the CO reducing capacity. At room temperature the main signals corresponding to Co_3O_4 at 691, 521, and 484 cm^{-1}, as well as the main signal of CeO_2 at 463 cm^{-1}, were detected (**Figure 5A**). As the temperature increased, the intensity of the Co_3O_4 bands decreased. However, a weak signal around 690 cm^{-1} was distinguished at 300°C, while at 325°C no signals of Co_3O_4 were detected, which implied that Co_3O_4 was completely reduced by CO from the gas phase. The catalyst was cooled to room temperature in 1% CO/Ar mixture and then maintained in Ar atmosphere.

The following experiment consisted in oxidizing the reduced catalyst with a 1% O_2/Ar stream, and the spectra are exhibited in **Figure 5B**. In the spectrum at the bottom, recorded at room temperature, it is possible to observe the main signal of CeO_2 at 463 cm^{-1}, as well as a broad signal between 500 and 600 cm^{-1}, which was assigned to oxygen vacancies. As the temperature increases, this broad band

decreases due to the incorporation of oxygen from the gas phase into the structure. Moreover, at 200°C the signals corresponding to Co_3O_4 are observable due to the oxidation of Co metal particles. After the experiment, the catalyst was cooled in 1% O_2/Ar flow at room temperature, and then it was treated in an Ar stream during several minutes. The corresponding spectrum registered at room temperature is shown in **Figure 5C**.

After that, the catalyst was again reduced at 350°C by a reducing stream (1% CO, 40% H_2 in Ar), and then, it was cooled in the same stream. A new spectrum was recorded at room temperature, and it is only possible to observe the main signal of CeO_2 at 464 cm^{-1}. Then, the catalyst was treated in Ar stream during several minutes, and oxygen vacancies were again detected.

Subsequently, the catalyst was subjected to a stream composed of the COPrOx reactant mixed gas flow (1% CO, 1% O_2, 40% H_2 and Ar). At room temperature the CeO_2 main signal was still observed. The temperature was increased, and at 150°C it was possible to detect a little band at 680 cm^{-1}, which belongs to Co_3O_4, which indicates that the oxygen present in the reactant gas stream is capable of reoxidizing the reduced cobalt species. When the temperature continued increasing, the band at 680 cm^{-1} was well defined, but at 300°C, it started again to decrease. At 325°C, the signal completely disappeared.

3.5 X-ray photoelectron spectroscopy

The surface characterization of Co-based catalysts was analyzed by the XPS technique, and the spectra for Co 2p and O 1s core levels are presented in **Figure 6**. The Co 2p spectrum shows two peaks at 780.1 and 795.0 eV, corresponding to the Co $2p_{3/2}$-Co $2p_{1/2}$ spin-orbit splitting (**Figure 6A**). These binding energies (BE) could be assigned to Co^{2+} or Co^{3+} species, since the BE difference is negligible for both species. However, the presence of intense satellite peaks is distinctive of the Co^{2+} spectrum [36, 37]. The cobalt spectra present very small satellite peaks, or else, the absence of them would indicate that Co^{3+} species are dominant for all catalysts.

Figure 6B shows the O 1s XP spectra for all of the catalysts studied. Broad and complex shape spectra are observed in this region. These spectra can be described as the result of the overlapping of two components corresponding to different

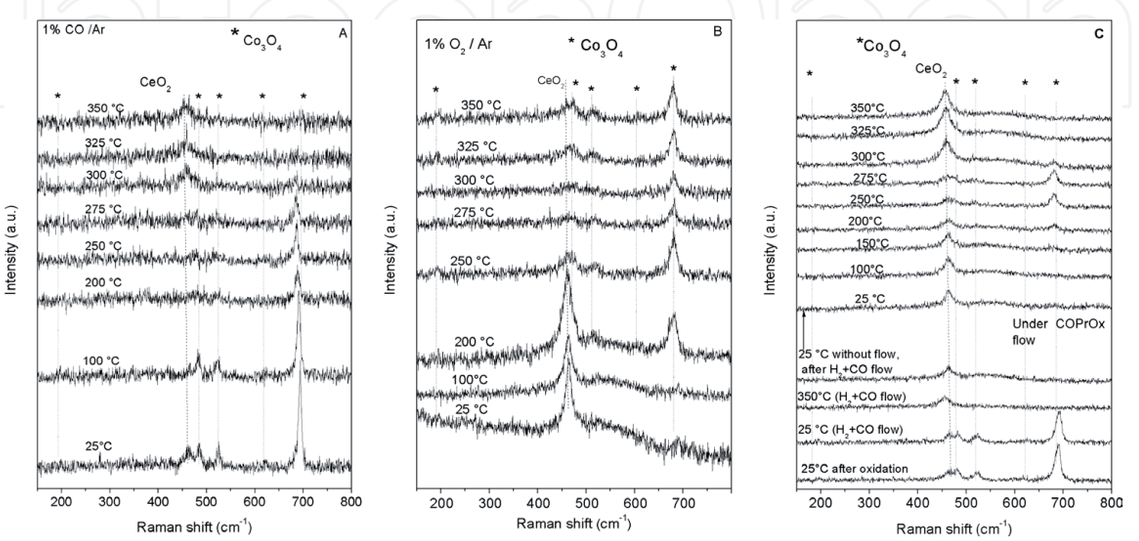

Figure 5.
In situ Raman study of CoCe-I. (A) 1% CO/Ar flow, (B) 1% O_2/Ar flow, and (C) under reaction conditions (1%CO, 1%O_2, 40% H_2, Ar).

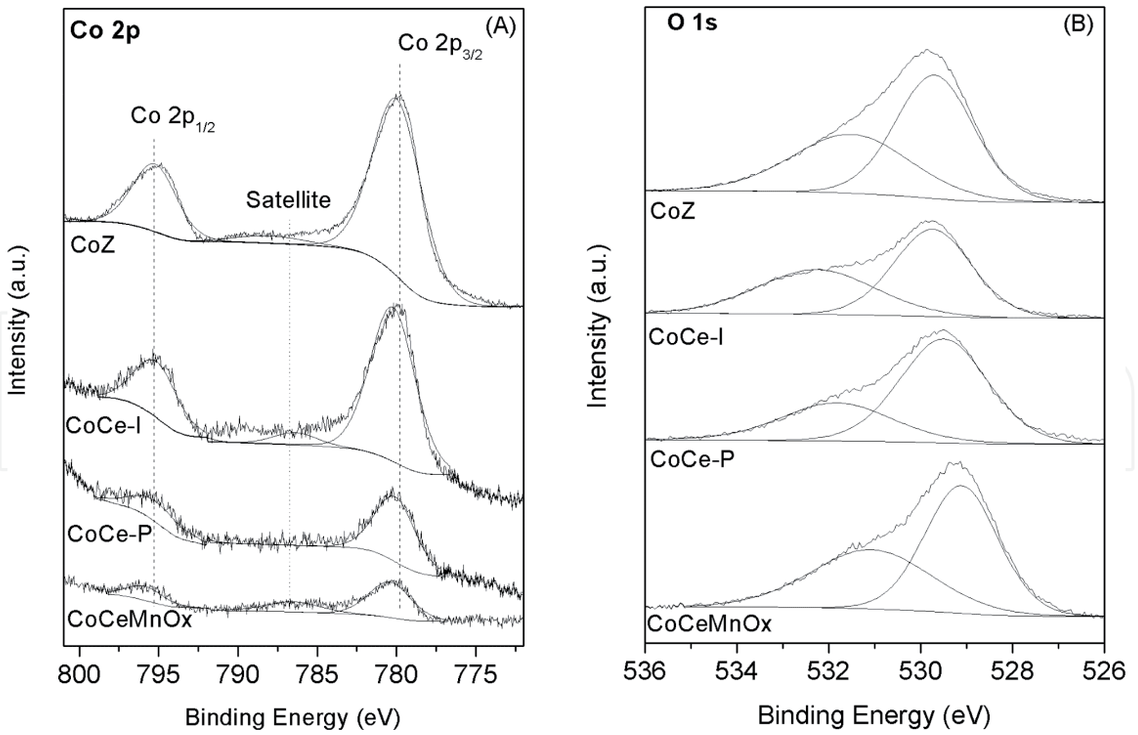

Figure 6.
XPS spectra of Co $2p_{3/2}$ (A) and O 1s (B) for CoZ, CoCe-I, CoCe-P, and CoCeMnOx catalysts.

species or groups of species. The first peak appears at 529.8 eV and the other at 532.3 eV. The oxygen signal at lower BE corresponds to bulk CeO_2 oxide and to cobalt oxides [38, 39]. The other component is assigned to hydroxyl, water, and/or carbonate groups adsorbed on the solid surface [40].

3.6 Catalytic evaluation

The COPrOx reaction system can be described by the following two reactions; the first one corresponds to CO oxidation, while the second one is the undesirable H_2 oxidation reaction.

$$CO + 0.5\ O_2 \rightarrow CO_2 \tag{5}$$

$$H_2 + 0.5\ O_2 \rightarrow H_2O \tag{6}$$

Figure 7A presents CO conversion curves of different catalysts as a function of temperature. It can be observed that the catalyst which was prepared with ZrO_2 support reached a conversion maximum (92%) lower than that reached by the catalysts prepared with cerium and at a higher temperature (200°C). CoCe-I and CoCe-P reached almost total CO conversion at 175 and 165°C, respectively, showing that CeO_2 is a better catalytic support than ZrO_2. Moreover, the small difference in catalytic performance which exists between CoCe-I and CoCe-P indicates that the coprecipitation method is slightly suitable to obtain an adequate catalyst for this reaction. When manganese was incorporated to the catalytic formulation, it could be observed that with the CoCeMnOx catalyst, complete CO conversion was reached at lower temperature than other catalysts. In addition, the temperature window of CO maxima conversion was maintained on a wide temperature range (150–200°C). **Figure 7B** shows the O_2 to CO_2 selectivity curves as a function of temperature. Selectivity curves exhibited a decreasing trend as the temperature

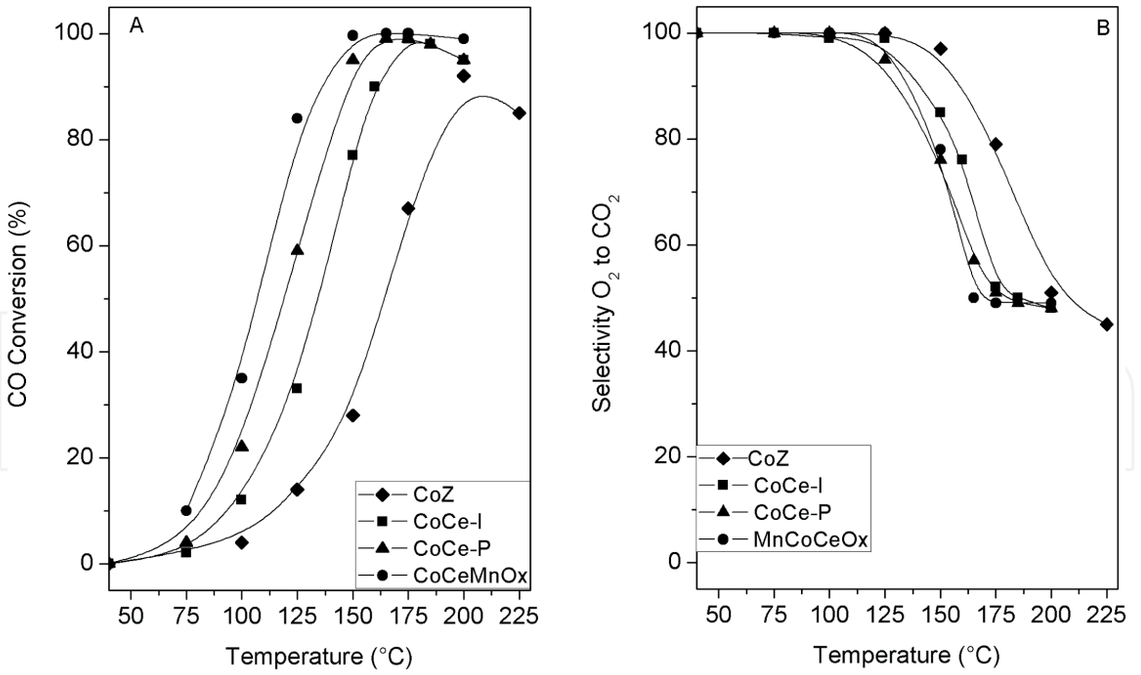

Figure 7.
COPrOx reaction on CoZ, CoCe-I, CoCe-P, and CoCeMnOx catalysts. (A) CO conversion (%). (B) O_2 selectivity to CO_2 (%). Reaction conditions: 1% CO, 1% O_2, 40% H_2 and He balance. W/F: 2.1 mg min/mL.

increased. Since the H_2 oxidation (reaction 2) had a higher apparent activation energy than the CO oxidation (reaction 1), as temperature increased, the hydrogen oxidation rate also increased so that CO conversion decreased and, consequently, the selectivity curve also decreased.

Moreover, the stability of CoCeMnOx and the effect of CO_2 adding in the feed were studied at 175°C during 75 h under reaction conditions. The CO conversion was maintained at 95% while the selectivity increased from 50 to 60%. The used catalysts did not show carbon formation by LRS spectroscopy.

The CeO_2 support with high mobility of surface lattice oxygen promotes the surface exchange between reduced and oxidized species $Ce^{4+} + Co^{2+} \leftrightarrow Ce^{3+} + Co^{3+}$. This process allows that the Co^{3+} species are available on the catalytic surface.

In the case of CoCeMnOx, which is the most active catalyst, the Co^{2+} species are oxidized by oxygen from Mn oxides or CeO_2 support, and then they are oxidized by oxygen from the gas phase. The redox couples Co^{2+}/Co^{3+} and Ce^{3+}/Ce^{4+} are improved by the presence of MnOx.

The in situ Raman results suggest that the active phase participates in the chemical reaction by a redox mechanism, where Co^{3+} oxidizes CO and reduces itself to Co^{2+}, but this cobalt species is permanently reoxidized by oxygen provided by CeO_2 and/or the gas phase. These experiments also allow inferring that the reduction step limits the overall reaction while the reoxidation on the surface is very fast.

4. Conclusions

The nature of cobalt species observed on Co-based catalysts used on the COPrOx reaction was influenced by the constituent species of the environment.

The XRD, TPR, XPS, and LRS characterizations showed that the Co_3O_4 active phase was present in all catalysts. From diffraction patterns of CoOx-ZrO_2 and the CoOx-CeO_2 catalysts, the Co_3O_4 spinel and the signals corresponding to ZrO_2 and CeO_2 were identified in agreement with laser-Raman spectra.

The CoCeMnOx catalyst, prepared by coprecipitation of precursor salts, showed an incipient development of a new phase $(Mn,Co)_3O_4$ mixed spinel, due to the intimate contact between elements.

The reduction of cobalt oxides was completed below 400°C and was promoted by the oxygen vacancies of ceria. In contrast, in the CoZ catalysts, the cobalt species were totally reduced at 440°C. The profiles showed two reduction steps assigned to Co^{3+} to Co^{2+} and then Co^{2+} to Co^0.

In situ laser-Raman spectroscopy revealed that cobalt species remained oxidized in spite of the reducing atmosphere of the reactant flow within the temperature range studied.

The XPS spectra showed the coexistence of Co^{2+} and Co^{3+} species according to the Co_3O_4 phase on the catalytic surface.

The CO conversion reached by the CoOx-CeO_2 catalysts was higher than the CoOx-ZrO_2 sample, due to redox properties of ceria. The manganese addition promoted the catalytic activity, widening the temperature window of maximum CO conversion.

Acknowledgements

The authors acknowledge the financial support received from UNL, ANPCyT, and CONICET. Thanks are given to Fernanda Mori for the XPS measurements.

Conflict of interest

The authors declare no conflict of interest with any person, institution, or organization for the publication of this chapter.

Author details

Leticia E. Gómez and Alicia V. Boix*
School of Chemical Engineering, Institute of Research on Catalysis and Petrochemistry (INCAPE), Universidad Nacional del Litoral (FIQ-UNL), Santa Fe, Argentina

*Address all correspondence to: aboix@fiq.unl.edu.ar

IntechOpen

© 2019 The Author(s). Licensee IntechOpen. This chapter is distributed under the terms of the Creative Commons Attribution License (http://creativecommons.org/licenses/by/3.0), which permits unrestricted use, distribution, and reproduction in any medium, provided the original work is properly cited.

References

[1] Abbott D. Keeping the energy debate clean: How do we supply the world's energy needs? Proceedings of the IEEE. 2010;**98**:42-66. DOI: 10.1109/JPROC.2009.2035162

[2] Baykara SZ. Hydrogen: A brief overview on its sources, production and environmental impact. International Journal of Hydrogen Energy. 2018;**43**:10605-10614. DOI: 10.1016/j.ijhydene.2018.02.022

[3] Brandon NP, Kurban Z. Clean energy and the hydrogen economy. Physical and Engineering Sciences. 2017;**375**:20160400. DOI: 10.1098/rsta.2016.0400

[4] Wang Y, Chen KS, Mishler J, Cho SC, Adroher XC. A review of polymer electrolyte membrane fuel cells: Technology, applications, and needs on fundamental research. Applied Energy. 2010;**88**:981-1007. DOI: 10.1016/j.apenergy.2010.09.030

[5] Bion N, Epron F, Moreno M, Mariño F, Duprez D. Preferential oxidation of carbon monoxide in the presence of hydrogen (PROX) over noble metals and transition metal oxides: Advantages and drawbacks. Topics in Catalysis. 2008;**51**:76-88. DOI: 10.1007/s11244-008-9116-x

[6] Park ED, Lee D, Lee HC. Recent progress in selective CO removal in a H_2-rich stream. Catalysis Today. 2009;**139**:280-290. DOI: 10.1016/j.cattod.2008.06.027

[7] Gómez LE, Sollier BM, Mizrahi M, Ramallo López JM, Miró EE, Boix AV. Preferential CO oxidation on Pt-Cu/Al_2O_3 catalysts with low Pt loadings. International Journal of Hydrogen Energy. 2014;**39**:3719-3729. DOI: 10.1016/j.ijhydene.2013.12.146

[8] Serra RM, Aspromonte SG, Miró EE, Boix AV. Hydrocarbon adsorption and NOx-SCR on (Cs,Co) mordenite. Applied Catalysis B: Environmental. 2015;**166-167**:592-602. DOI: 10.1016/j.apcatb.2014.11.061

[9] Banús ED, Milt VG, Miró EE, Ulla MA. Catalytic coating synthesized onto cordierite monolith walls. Its application to diesel soot combustión. Applied Catalysis B: Environmental. 2013;**132-133**:479-486. DOI: 10.1016/j.apcatb.2012.12.020

[10] Coronel L, Múnera JF, Tarditi AM, Moreno MS, Cornaglia LM. Hydrogen production by ethanol steam reforming over Rh nanoparticles supported on lanthana/silica systems. Applied Catalysis B: Environmental. 2014;**160-161**:254-266. DOI: 10.1016/j.apcatb.2014.05.025

[11] Dalla Fontana A, Faroldi B, Cornaglia LM, Tarditi A. Development of catalytic membranes over PdAu selective films for hydrogen production through the dry reforming of methane. Molecular Catalysis. DOI: 10.1016/j.mcat.2018.07.018

[12] Gómez LE, Tiscornia IS, Boix AV, Miró EE. Co/ZrO_2 catalysts coated on cordierite monoliths for CO preferential oxidation. Applied Catalysis A: General. 2011;**401**:124-133. DOI: 10.1016/j.apcata.2011.05.007

[13] Gómez LE, Tiscornia IS, Boix AV, Miró EE. CO preferential oxidation on cordierite monoliths coated with Co/CeO_2 catalysts. International Journal of Hydrogen Energy. 2012;**37**:14812-14819. DOI: 10.1016/j.ijhydene.2012.01.159

[14] Banús ED, Ulla MA, Miró EE, Milt VG. Co,Ba,K/ZrO_2 coated onto metallic foam (AISI 314) as a structured catalyst for soot combustion: Catalytic activity and stability. Applied Catalysis A: General. 2011;**393**:9-16. DOI: 10.1016/j.apcata.2010.11.018

[15] Boix AV, Aspromonte SG, Miró EE. Deactivation studies of the SCR of NOx with hydrocarbons on Co-mordenite monolithic catalysts. Applied Catalysis A: General. 2008;**341**:26-34. DOI: 10.1016/j.apcata.2007.12.032

[16] Gómez LE, Boix AV, Miró EE. Co/ZrO_2, Co/CeO_2 and MnCoCe structured catalysts for COPrOx. Catalysis Today. 2013;**216**:246-253. DOI: 10.1016/j.cattod.2013.05.010

[17] Liu K, Wang A, Zhang T. Recent advances in preferential oxidation of CO reaction over platinum group metal catalysts. ACS Catalysis. 2012;**2**:1165-1178. DOI: 10.1021/cs200418w

[18] Komatsu T, Takasaki M, Ozawa K, Furukawa S, Muramatsu A. PtCu intermetallic compound supported on alumina active for preferential oxidation of CO in hydrogen. Journal of Physical Chemistry C. 2013;**117**:10483-10491. DOI: 10.1021/jp4007729

[19] Korotkikh O, Farrauto R. Selective catalytic oxidation of CO in H_2: Fuel cell applications. Catalysis Today. 2000;**62**:249-254. DOI: 10.1016/S0920-5861(00)00426-0

[20] Marbán G, Fuertes AB. Highly active and selective CuOx/CeO_2 catalyst prepared by a single-step citrate method for preferential oxidation of carbon monoxide. Applied Catalysis B: Environmental. 2005;**57**:43-53. DOI: 10.1016/j.apcatb.2004.10.011

[21] Jampa S, Wangkawee K, Tantisriyanurak S, Changpradit J, Jamieson AM, Chaisuwan T, et al. High performance and stability of copper loading on mesoporous ceria catalyst for preferential oxidation of CO in presence of excess of hydrogen. International Journal of Hydrogen Energy. 2017;**42**:5537-5548. DOI: 10.1016/j.ijhydene.2016.08.078

[22] Lacoste AM, Tiscornia IS, Boix AV. CO preferential oxidation on cordierite monoliths coated with CuO-CeO_2/SBA-15 catalysts. Further insights into the physico-chemical aspects of the catalytic behavior. International Journal of Hydrogen Energy. 2018;**43**:14238-14251. DOI: 10.1016/j.ijhydene.2018.05.122

[23] Liotta LF, Di Carlo G, Pantaleo G, Venezia AM, Deganello G. Co_3O_4/CeO_2 composite oxides for methane emissions abatement: Relationship between Co_3O_4-CeO_2 interaction and catalytic activity. Applied Catalysis B: Environmental. 2006;**66**:217-227. DOI: 10.1016/j.apcatb.2006.03.018

[24] Gómez LE, Múnera JF, Sollier BM, Miró EE, Boix AV. Raman in situ characterization of the species present in Co/CeO_2 and Co/ZrO_2 catalysts during the COPrOx reaction. International Journal of Hydrogen Energy. 2016;**41**:4993-5002. DOI: 10.1016/j.ijhydene.2016.01.099

[25] Zhao Z, Jin R, Bao T, Yang H, Lin X, Wang G. Mesoporous $Ce_xMn_{1-x}O_2$ composites as novel alternative carriers of supported Co_3O_4 catalysts for CO preferential oxidation in H_2 stream. International Journal of Hydrogen Energy. 2012;**37**:4774-4786. DOI: 10.1016/j.ijhydene.2011.12.057

[26] Zhao Z, Lin X, Jin R, Wang G, Muhammad T. MOx (M=Mn, Fe, Ni or Cr) improved supported Co_3O_4 catalysts on ceria-zirconia nanoparticulate for CO preferential oxidation in H_2-rich gases. Applied Catalysis B: Environmental. 2012;**115-116**:53-62. DOI: 10.1016/j.apcatb.2011.12.001

[27] Gómez LE, Miró EE, Boix AV. Spectroscopic characterization of Mn-Co-Ce mixed oxides, active catalysts for COPROX reaction. International Journal of Hydrogen Energy. 2013;**38**:5645-5654. DOI: 10.1016/j.ijhydene.2013.03.004

[28] Picasso G, Gutiérrez M, Pina MP, Herguido J. Preparation and characterization of Ce-Zr and Ce-Mn based oxides for n-hexane combustion: Application to catalytic membrane reactors. Chemical Engineering Journal. 2007;**126**:119-130. DOI: 10.1016/j.cej.2006.09.005

[29] Trovarelli A. Catalytic properties of ceria and CeO_2-containing materials. Catalysis Reviews: Science and Engineering. 1996;**38**(4):439-520. DOI: 10.1080/01614949608006464

[30] Luo JY, Meng M, Li X, Li XG, Zha YQ, Hu TD, et al. Mesoporous Co_3O_4-CeO_2 and Pd/Co_3O_4-CeO_2 catalysts: Synthesis, characterization and mechanistic study of their catalytic properties for low-temperature CO oxidation. Journal of Catalysis. 2008;**254**:310-324. DOI: 10.1016/j.jcat.2008.01.007

[31] Wu Z, Li M, Howe J, Meyer HM, Overbury SH. Probing defect sites on CeO_2 nanocrystals with well-defined surface planes by Raman spectroscopy and O_2 adsorption. Langmuir. 2010;**26**:16595-16606. DOI: 10.1021/la101723w

[32] Zdravković J, Simović B, Golubović A, Poleti D, Veljković I, Šćepanović M, et al. Comparative study of CeO_2 nanopowders obtained by the hydrothermal method from various precursors. Ceramics International. 2015;**41**:1970-1979. DOI: 10.1016/j.ceramint.2014.08.122

[33] Lee Y, He G, Akey A, Si R, Flytzani-Stephanopoulos M, Herman IP. Raman analysis of mode softening in nanoparticle $CeO_{2-\delta}$ and Au-$CeO_{2-\delta}$ during CO oxidation. Journal of the American Chemical Society. 2011;**133**:12952-12955. DOI: 10.1021/ja204479j

[34] Woods MP, Gawade P, Tan B, Ozkan US. Preferential oxidation of carbon monoxide on Co/CeO_2 nanoparticles. Applied Catalysis B: Environmental. 2010;**97**:28-35. DOI: 10.1016/j.apcatb.2010.03.015

[35] Tang CW, Wang CB, Chien SH. Characterization of cobalt oxides studied by FT-IR, Raman, TPR and TG-MS. Thermochimica Acta. 2008;**473**:68-73. DOI: 10.1016/j.tca.2008.04.015

[36] Hagelin-Weaver HAE, Hoflund GB, Minahan DM, Salaita GN. Electron energy loss spectroscopic investigation of Co metal, CoO, and Co_3O_4 before and after Ar^+ bombardment. Applied Surface Science. 2004;**235**:420-448. DOI: 10.1016/j.apsusc.2004.02.062

[37] Pietrogiacomi D, Tuti S, Campa MA, Indovina V. Cobalt supported on ZrO_2: Catalysts characterization and their activity for the reduction of NO with C_3H_6 in the presence of excess O_2. Applied Catalysis B: Environmental. 2000;**28**:43-54. DOI: 10.1016/S0926-3373(00)00161-2

[38] Liu J, Zhao Z, Wang J, Xu C, Duan A, Jiang G, et al. The highly active catalysts of nanometric CeO_2-supported cobalt oxides for soot combustion. Applied Catalysis B: Environmental. 2008;**84**:185-195. DOI: 10.1016/j.apcatb.2008.03.017

[39] Galtayries A, Sporken R, Riga J, Blanchard G, Caudano R. XPS comparative study of ceria/zirconia mixed oxides: Powders and thin film characterization. Journal of Electron Spectroscopy and Related Phenomena. 1998;**88-91**:951-956. DOI: 10.1016/S0368-2048(97)00134-5

[40] Alvarez M, López T, Odriozola JA, Centeno MA, Domínguez MI, Montes M, et al. 2,4-Dichlorophenoxyacetic acid (2,4-D) photodegradation using an Mn^+/ZrO_2photocatalyst: XPS, UV-vis, XRD characterization. Applied Catalysis B: Environmental. 2007;**73**:34-41. DOI: 10.1016/j.apcatb.2006.12.010